The Paleocene-Eocene Thermal Maximum at DSDP Site 277, Campbell Plateau, southern Pacific Ocean

C.J. Hollis[1], B.R. Hines[2], K. Littler[3,4], V. Villasante-Marcos[5], D.K. Kulhanek[6], C.P. Strong[1], J. C. Zachos[3], S.M. Eggins[7], L. Northcote[8], A. Phillips[1]

[1] GNS Science, PO Box 30-368, Lower Hutt 5040, New Zealand
[2] School of Geography, Environment & Earth Sciences, Victoria University of Wellington, New Zealand
[3] Earth & Planetary Sciences, University of California – Santa Cruz, California 95060, USA
[4] Camborne School of Mines, University of Exeter, Penryn Campus, Cornwall, TR10 9FE, UK
[5] Observatorio Geofísico Central, Instituto Geográfico Nacional, 28014 Madrid, Spain
[6] International Ocean Discovery Program, Texas A&M University, College Station, TX 77845-9547, USA
[7] Research School of Earth Sciences, The Australian National University, Canberra 0200, ACT, Australia
[8] National Institute of Water and Atmosphere, PO Box 14901, Wellington, New Zealand

ABSTRACT

Re-examination of sediment cores from Deep Sea Drilling Project (DSDP) Site 277 on the western margin of the Campbell Plateau (paleolatitude of ~65°S) has identified an intact Paleocene-Eocene (P-E) boundary overlain by a 34 cm-thick record of the Paleocene-Eocene Thermal Maximum (PETM) within nannofossil chalk. The upper part of the PETM is truncated, either due to drilling disturbance or a sedimentary hiatus. An intact record of the onset of the PETM is indicated by a gradual decrease in $\delta^{13}C$ values over 20 cm, followed by a 14 cm interval in which $\delta^{13}C$ is 2‰ lighter than uppermost Paleocene values. After accounting for effects of diagenetic alteration, we use $\delta^{18}O$ and Mg/Ca values from foraminiferal tests to determine that intermediate and surface waters warmed by ~5-6° at the onset of the PETM prior to the full development of the negative $\delta^{13}C$ excursion. After this initial warming, sea temperatures were relatively stable through the PETM, but declined abruptly across the horizon that truncates the event at this site. Mg/Ca analysis of foraminiferal tests indicate peak intermediate and surface water temperatures of ~19°C and ~32°C, respectively. These

temperatures may be influenced by residual diagenetic factors, changes in ocean circulation, and surface water values may also be biased towards warm season temperatures.

1. Introduction

Stable isotope analysis of foraminiferal tests from sediments cored at DSDP Site 277 (Shackleton and Kennett, 1975) provided the first paleotemperature record for the Paleogene of the Southern Ocean and laid the foundation for many subsequent studies of the regional paleoclimate and paleoceanography (e.g., Kennett 1977, 1980; Kennett and Shackleton, 1976; Hornibrook, 1992; Nelson and Cook, 2001). Over the last decade, there has been renewed interest in the early Paleogene (66 to 35 Ma) climate history of the Southern Ocean, partly driven by a societal imperative to understand how the Antarctic ice sheet will respond to anthropogenic global warming (e.g., Joughin et al., 2014). The early Paleogene was the last time that Earth is inferred to have experienced greenhouse gas levels in excess of ~600 ppm CO_2 (Zachos et al., 2008; Beerling and Royer, 2011), and therefore provides insight into a climate state that civilization may experience in coming centuries. One event in particular has been touted as a geological analogue for greenhouse gas-driven global warming: the Paleocene-Eocene Thermal Maximum (PETM, ~56 Ma). This event was a short-lived (~220 kyrs) perturbation to the climate and carbon cycle in which global temperatures rose by 4–5°C within a few thousand years (Sluijs et al., 2007; McInerney and Wing, 2011; Dunkley-Jones et al., 2013; Schmidt, 2014), with warming of up to 8°C in higher latitudes and some coastal settings (Thomas et al., 2002; Sluijs et al., 2006, 2011; Zachos et al., 2006; Hollis et al., 2012; Frieling et al., 2014). Multiple lines of evidence suggest that this warming may have been driven by a rapid injection of greenhouse gases, possibly sourced from submarine gas hydrates, as evidenced by coupled negative excursions in oxygen and carbon isotopes (Dickens et al., 1995, 1997). Several other potential sources of the light carbon have also been implicated to account for all or part of the carbon isotope ($\delta^{13}C$) excursion (Dickens, 2003, 2011; Kent et al., 2003; Svensen et al., 2004; Higgins and Schrag, 2006; De Conto et al., 2012).

The PETM has been identified in several sites in the Southwest Pacific, including onshore records in both siliciclastic and pelagic bathyal sections in eastern New Zealand (Kaiho et al., 1996; Crouch et al., 2001; Hancock et al., 2003; Hollis et al., 2005a, b, 2012; Nicolo et al., 2010), non-marine to marginal marine sediments in western New Zealand (Handley et al., 2011) and in shelfal sediments at Ocean Drilling Program (ODP) Site 1172, offshore eastern Tasmania (Sluijs et al., 2011). Here we report a new record of the PETM in pelagic bathyal sediments at DSDP Site 277, at a similar paleolatitude to Site 1172 (~65°S). These two sites represent the southernmost records of the PETM in the Pacific Ocean (Fig. 1).

Initial studies of Site 277 suggested that the Paleocene-Eocene (P-E) boundary occurred within a gap between cores 43 and 44 (Kennett et al., 1975). A subsequent biostratigraphic review of the site (Hollis et al., 1997) revealed that the boundary was lower in the drillhole, potentially within a relatively continuous interval preserved in core 45. Detailed re-sampling confirmed the location of the P-E boundary (Fig. 2), based on the highest occurrence (HO) of benthic foraminifer *Stensionina beccariformis* at 457.3 mbsf (277-45-3, 80 cm). High resolution stable isotope analysis of bulk carbonate confirms that this horizon marks the base of a 34 cm-thick negative excursion in $\delta^{13}C$ (CIE) that defines the PETM (Aubry et al., 2007).

DSDP Site 277 was drilled on the western margin of the Campbell Plateau in a water depth of 1214 m as part of DSDP Leg 29 (Kennett et al., 1975). Paleogene sedimentation occurred in fully oceanic conditions well above the lysocline (Kennett et al., 1975), with benthic foraminiferal assemblages indicating lower to middle bathyal water depths since the Paleocene (Hollis et al., 1997). In order to identify the paleoceanographic changes associated with the PETM at this site we have undertaken a multidisciplinary study that includes foraminiferal and calcareous nannofossil biostratigraphy, magnetic susceptibility, $CaCO_3$ content, elemental abundance using X-ray fluorescence (XRF), $\delta^{13}C$ and $\delta^{18}O$ analysis of bulk carbonate and foraminifera, and single test analysis of foraminifera for Mg/Ca ratios by Laser Ablation Inductively Coupled Plasma Mass Spectrometry (LA-ICPMS).

2. Material and Methods

2.1. Material

We analysed samples over a 45-m interval spanning the upper Paleocene to lower Eocene at DSDP Site 277 (470–425 mbsf). Average sample spacing was 20 cm over much of the interval, with a higher resolution of 2–3 cm sampling across the PETM within core-section 45-3 (~457.30–456.95 mbsf). In addition, this core-section was scanned for elemental abundance. Although the PETM interval is preserved, the overall record is discontinuous, with significant gaps between cores from core 42 to 45 (Fig. 2).

2.2. Methods

2.2.1. X-Ray fluorescence (XRF) core scanning

XRF data were acquired using an Avaatech XRF scanner with a Canberra X-PIPS silicon drift detector, model SXD 15C-150-500 150 eV resolution X-ray detector, which is housed at the International Ocean Discovery Program (IODP) Gulf Coast Repository at Texas A&M University in College Station, Texas (Table S1). This scanner is configured for analysis of split core section halves, with the X-ray tube and detector mounted on a moving track (Richter et al., 2006). Section 277-45-3 was removed from the core refrigerator and allowed to equilibrate to room temperature prior to analysis. We levelled all rock pieces within the section, as the detector requires a flush surface with no gaps between pieces, and then covered the section with 4 µm thick Ultralene plastic film (SPEX Centriprep, Inc.) to protect the detector. The section was scanned at 2 mm intervals using a voltage of 10 kV for elements Al, Si, P, S, Cl, Ar, K, Ca, Ti, Cr, Mn, Fe, Rh, and Ba. The scan was completed using a 1 mA tube current, no filter, and a detector live time of 30 s, with an X-ray detection area of 2 mm in the downcore direction and 15 mm across the core. During measurement, intervals were skipped where gaps of more than ~2 mm existed between pieces. Smaller gaps were noted so that suspect data across these gaps could be removed.

2.2.2. Rock magnetism

Bulk magnetic susceptibility of a subset of discrete samples was measured at the Paleomagnetism Laboratory of the Complutense University of Madrid, Spain (Table S2). A KLY-4 (Agico) susceptibility bridge was employed, with an applied magnetic field of 300 A/m. Due to the low ferromagnetic content of most samples, each sample was measured ten times and averaged. The error bars of the magnetic susceptibility data correspond to the standard deviation of the mean (1σ) obtained during the averaging procedure.

2.2.3. Micropaleontology

Calcareous nannofossil and foraminifera sample preparation and examination followed standard procedures. Samples for calcareous nannofossils were prepared using standard smear-slide techniques (Bown and Young, 1998). A small amount of sediment was mixed with a drop of water on a coverslip, distributed with a toothpick, and then dried on a hot plate. The coverslip was affixed to a glass microscope slide using Norland Optical Adhesive 61 and cured under an ultraviolet light. Slides were examined on a Leitz Ortholux II POL-BK microscope under cross-polarized and plane-transmitted light. Nannofossil distribution was determined for 41 samples extending from Paleocene to the upper lower Eocene (Teurian to Mangaorapan New Zealand stages) (Table S3). Counts of 400 specimens were conducted at 1000× for each sample, followed by a scan of at least 400 fields of view at 630× to look for rare taxa). Foraminiferal distribution was determined for 59 samples spanning the same time interval (Table S4).

Foraminiferal biostratigraphy is correlated with New Zealand stages (Cooper, 2004) and international biozones (Olsson et al., 1999; Pearson et al., 2006). New Zealand stage and biozone boundaries are calibrated to the 2012 geological timescale (Gradstein et al., 2012) using criteria described by Raine et al. (2015) and Norris et al. (2014). Foraminiferal taxonomy is based on Hornibrook et al. (1989). Biostratigraphic results for calcareous nannofossils are correlated to the biostratigraphic zonation scheme of Martini (1970, 1971), calibrated to the 2012 geological timescale (Gradstein et al., 2012). Taxonomic concepts for species are those given in Perch-Nielsen (1985) and Bown (1998).

2.2.4. Stable isotopes and carbonate content

Analysis for stable isotopes and carbonate content was undertaken at three laboratories. Results are tabulated in Table S5. Bulk carbonate $\delta^{13}C$ and $\delta^{18}O$ measurements were undertaken at the National Isotope Centre, GNS Science, Lower Hutt. Samples were analysed on the GVI IsoPrime Carbonate Preparation System at a reaction temperature of $25^{o}C$ and run via dual inlet on the IsoPrime mass spectrometer. All results are reported with respect to VPDB, normalized to the GNS marble internal standard with reported values of 2.04‰ for $\delta^{13}C$ and -6.40‰ for $\delta^{18}O$. The external precision (1σ) for these measurements is 0.05‰ for $\delta^{13}C$ and 0.12‰ for $\delta^{18}O$.

Individual specimens from five foraminiferal genera were used for stable isotope analysis and elemental geochemistry. Specimens were selected for analysis based on visual assessment of their preservation under a stereo microscope. Wherever possible, analyses were performed on *Morozovella aequa*, *Acarinina coalingensis*, *Subbotina patagonica*, *S. roesnasensis*, and *Cibicides proprius/praemundus, and Stensioina beccariformis*. The following species were substituted when these species were not available: *Morozovella subbotinae, M. acuta, M. apanthesma, Acarinina soldadoensis, A subsphaerica, A. esnaensis, A. nitida and Cibicides tholus*. The stable isotope signature of *Acarinina soldadoensis, A subsphaerica, A. nitida* and all species of *Morozovella* indicates they were mixed layer dwellers (Olsson et al., 1999; Quillévéré and Norris, 2003), and therefore are appropriate indicators of near surface conditions. *Subbotina patagonica* is inferred to have had a deeper planktonic habitat (Pearson et al., 2006), within the thermocline. There is no data on the habitat *of S. roesnasensis*.Stable isotope analysis of foraminifera was carried out in the Stable Isotope Laboratory at the University of California, Santa Cruz. Between 1 and 6 (average of 3) specimens of *Cibicides*, 1 and 5 (average of 3) specimens of *Stensioina*, 3–17 (average of 10) specimens of *Acarinina*, 2–10 (average of 4) specimens of *Morozovella*, and 1–8 (average of 5) specimens of *Subbotina* were used in each analysis. Specimens were first sonicated in deionised water to remove clay and detrital calcite. Isotopic measurements were carried out on a Thermo-Finnigan MAT253 mass spectrometer interfaced with a Kiel Device. The analytical precision (1σ) is based on repeat analysis of an in-house standard (Carrara marble), calibrated to the international standards NBS18 and NBS19, and averages ±0.05 ‰ for $\delta^{13}C$ and ±0.08 ‰ for $\delta^{18}O$. All values are reported relative to VPDB. For the δ^{18}O values of *Cibicides* (= *Cibicidoides*; see Schweizer et al., 2009) and *Stensioina*, we apply an isotopic correction factor of +0.28 (Katz et al., 2003). Paleotemperatures for both benthic and planktic taxa were calculated from δ^{18}O using the equation of Kim and O'Neil (1997):

$$T\,(^{\circ}C) = 16.1 + -4.64(\delta^{18}O_M - \delta^{18}O_{SW}) + 0.09(\delta^{18}O_M - \delta^{18}O_{SW})^2$$

Equation 1

Where $\delta^{18}O_M$ = measured value and $\delta^{18}O_{SW}$ = -1.23‰, which is the inferred value for sea water under ice-free conditions (assuming ice-free ocean values of = -1‰). Planktic values are also corrected for for paleolatitude (Zachos et al. 1994; correction of -0.23‰).

The carbonate content of dried powdered samples was determined at the National Institute of Water and Atmosphere (NIWA, Wellington) via gasometric quantitative analysis after acidification (Jones and Kaiteris, 1983), with a precision of ±2%.

2.2.5. Elemental geochemistry and Mg/Ca analysis

Foraminifera were picked from the 150–300 µm fraction of washed sediment samples and individually washed in ultra-pure (>18.2 mΩ) water and analytical grade methanol three times before being mounted on double-sided tape adhered to a glass slide. Mg/Ca analysis was carried out on 4–19 specimens for each of the selected genera in each sample (Table S6). Each foraminifer was analysed at least three times using a pulsed Ar-F excimer laser (Lambda Physik LPFpro 205) with a 193 µm wavelength, 30 µm spot size, laser power of 3 J/cm^2 and a repetition rate of 3 Hz, in conjunction with an ANU HelEx laser ablation cell, at the Research School of Earth Sciences of the Australian National University. An analysis of the NIST-SRM610 silicate standard was taken between every 9–12 foraminifer analyses to correct for elemental fractionation originating from laser ablation and mass-spectrometry effects.

The final three chambers of the final whorl in each specimen were analysed individually by ablating slowly at a rate of 0.2–0.3 µms^{-1} to produce a separate trace element profile through the wall of each chamber (Fig. S1). A Varian 820 ICPMS was used to measure abundances of the trace metal isotopes ^{24}Mg, ^{27}Al, ^{29}Si, ^{47}Ti, ^{55}Mn, ^{66}Zn, ^{88}Sr and ^{138}Ba relative to ^{43}Ca during ablation. Elemental ratios reported for each sample are average values derived from multiple screened profile segments for multiple specimens of a given taxon. Laser ablation sites were selected using light microscopy and SEM imaging to avoid zones of detrital contamination, recrystallization or test ornamentation that might cause irregular trace element/Ca profiles (Fig. S1). Individual chamber profiles were screened to exclude zones with anomalously high Mg/Ca, Al/Ca, Mn/Ca or Ba/Ca ratios, which indicate significant silicate contamination (Barker et al., 2003; Greaves et al., 2005;

Creech et al., 2010). These profiles typically show zones of enriched in Mg, Al, Mn, and Ba on the outside and inside surfaces of the chamber wall, consistent with silicate contamination (Fig. S1). The Sr/Ca ratio is used as an indicator of diagenetic alteration because the concentration of Sr may decrease or increase during alteration or secondary calcification (Eggins et al., 2003; Kozdon et al., 2013). A ratio of ~1.4 is typical for well-preserved tests (Creech et al., 2010). Therefore, samples with Sr/Ca values outside the range of 0.8–1.6 mmol/mol were considered to be affected by diagenesis (Fig. 3). Al/Ca and Mg/Ca data show a positive linear correlation when plotted (Fig. 3), reflecting the influence of silicate contamination. We have used the method of Creech (2010; after Barker et al., 2003) to screen for this contamination. The Al/Mg composition of the contaminant phase was identified by plotting Mg/Ca against Al/Ca and finding the slope of the linear regression. Once this Al/Mg composition had been determined for each genus, the screening threshold was set by calculating the Al/Ca ratio at which paleotemperature estimates would be biased by more than 1 °C. This screening removes anomalously high Mg/Ca values and reduces the mean value for most samples (Fig. 4, S2). After the measurements have been screened for silicate contamination, the effects of diagenesis are more easily assessed (Fig. 3). A weak negative correlation between Sr/Ca and Mg/Ca suggests that diagenesis may also cause an increase in Mg/Ca values, especially in the planktic genus *Acarinina*. The reasons for this correlation and implications are discussed below.

Marine paleotemperatures are calculated using the exponential relationship between Mg/Ca and temperature (*Equation 2*). Because the planktic foraminifera used in this study are extinct, sea surface temperatures (SSTs) were calculated using a general calibration based on the mean calcification temperatures of nine modern planktic species (A = 0.09, B = 0.38; Anand et al., 2003). Sea floor temperatures (SFTs) were calculated using the calibration of Lear et al. (2002) based on three benthic species of *Cibicidoides/Cibicides* (A = 0.109, B = 0.867).

$$Mg/Ca_{test} = \left(\frac{Mg/Ca_{sw}^{t=t}}{Mg/Ca_{sw}^{t=1}}\right) \times Bexp^{AT}$$

Equation 2

Marine temperature reconstructions based on early Eocene foraminiferal calcite have shown that a high (>3 mol/mol) Mg/Ca_{sw} value is required to reconcile Mg/Ca-derived paleotemperatures with those derived from $\delta^{18}O$ (Lear et al., 2002; Sexton et al., 2006). High Mg/Ca_{sw} values are in line with modelled values from Wilkinson & Algeo (1989) but are at odds with several proxy studies (e.g., Horita et al., 2004; Coggon et al., 2010) and more recent modelling (e.g., Stanley & Hardie, 1998) that favour lower values for Mg/Ca_{SW} (<2 mol/mol). However, recent studies (Hasuik & Lohmann, 2010, Evans & Müller, 2012) have reconciled the empirical relationship between $\delta^{18}O$ and Mg/Ca paleotemperatures with these lower values for Mg/Ca_{SW} by showing that a power law distribution, rather than an exponential distribution, better describes the relationship between Mg-partitioning and temperature in foraminiferal calcite (*Equation 3*).

$$Mg/Ca_{test} = \left(\frac{B}{Mg/Ca_{sw}^{t=0^{H}}}\right) \times Mg/Ca_{sw}^{t=t^{H}} exp^{AT}$$

Equation 3

To apply this equation we use exponential and pre-exponential calibration constants from modern multispecies calibrations and paleotemperature values derived from oxygen isotopes to estimate the function *H* for extinct foraminifera. Published data from well-preserved Eocene foraminifera at Hampden Beach (Burgess et al., 2008; Hollis et al., 2012) and Tanzania (Pearson et al., 2007), for which paired Mg/Ca and $\delta^{18}O$ data is available, have been used to derive *H* for the extinct species used in this study.

In calculating the value of *H*, we have used an early Eocene Mg/Ca$_{sw}$ value of 1.6 mol/mol (Stanley & Hardie, 1998; Evans & Müller, 2012) and a modern Mg/Ca$_{sw}$ value of 5.17 mol/mol. This *H* value does not take into account possible variability in Mg/Ca$_{sw}$ values through the early Paleogene. The Mg/Ca-temperature calibrations of Anand et al. (2003) and Lear et al. (2002) have been used, although it is likely that the pre-exponential constant of Paleogene planktic foraminifera differed from that of the modern taxa. We calculate an H value of 20 for Paleogene planktic foraminifera, which is significantly lower than H values for modern planktics, such as *Globigerina sacculifer* (*H* = 0.42; Hasuik & Lohmann, 2010). For benthic foraminifera, Cramer et al. (2011) suggest that the value of *H* would be similar between *Cibicides* sp. and *Oridorsalis umbonatus*. Mg/Ca-derived temperature values are calculated using *Equation 4*.

$$T = \frac{\ln\left(\frac{[Mg/Ca_{test}] \times [Mg/Ca_{sw}^{t=0}]^{H}}{B \times [Mg/Ca_{sw}^{t=t}]^{H}}\right)}{A}$$

Equation 4

Temperature values derived from Mg/Ca ratios of surface mixed-layer dwelling taxa used in this study are normalised to *Morozovella crater* following Creech et al. (2010).

Three types of error are applied to paleotemperatures derived from Mg/Ca ratios; the analytical error, sample error and a standard calibration error. The analytical error is accounted for in the data processing step, and typically produces very small uncertainties (± 1–3% 2se) associated with counting statistics during ablation and data acquisition. The sample error pertains to the 95% confidence interval calculated for the mean temperature value obtained from multiple analyses within a single sample, and is calculated by:

$$\bar{X} \pm t \times \frac{\sigma}{\sqrt{n}}$$

Equation 5

Where $\bar{x}$ is the sample mean, t is the inverse of the Students' t-distribution, σ represents the standard deviation and n is the number of analyses. The calibration error is the residual error of ±1.6°C on the regression of the multispecies calibrations established by Lear et al. (2002) and Anand et al. (2003). The cumulative error calculated from the sum of all three errors is applied to each temperature value, providing upper and lower uncertainties.

3. Results and Discussion

3.1 Stratigraphy

The 45 m-thick studied interval (425−470 mbsf) consists of five cores, with significant gaps due to poor recovery in three of the cores, which extend from middle Paleocene to lower Eocene (Fig. 2). The sediments are greenish-white to greenish-grey nannofossil chalk, with higher clay content in the upper Paleocene (core 46; 463−470 mbsf) and lowermost Eocene (core section 45-3; 456.96−457.3 mbsf)) and minor glauconite (cores 43-44) and chert nodules (cores 41-43) in the overlying Eocene. A record of "incipient chert" in core section 45−3 (Kennett et al., 1975) may have been a misidentification of the darker-grey clay-rich sediments at the base of the PETM (Fig. 5).

Calcareous microfossils are only moderately preserved overall, and there is an interval directly below the Paleocene-Eocene boundary (457.3 to 457.58 mbsf) in which foraminifera are poorly preserved and sparse. Planktic foraminifera are used to correlate the 45 m-thick studied interval to New Zealand stages (Teurian to Mangaorapan) and to international foraminiferal zones P4a-b to E7 (Fig. 2). Nannofossil assemblages over the same interval have been correlated with nannofossil zones NP6 to NP12. Whereas previous studies indicated an undifferentiated upper Paleocene succession spanning Zone NP6–8 (Edwards and Perch-Nielsen, 1975; Hollis et al., 1997), we infer a ~2 Myr hiatus near the top of Core 46 (463.49–463.16 mbsf), representing all of zones NP7 and NP8. Immediately above the hiatus, *Discoaster multiradiatus* makes up ~2% of the assemblage, suggesting that the lowermost part of Zone NP9 is missing. This lowest occurrence (LO) of D. multiradiatus coincides with the LOs of *D. lenticularis* and *D. salisburgensis*.

The PETM is a 34 cm-thick interval within core 45 (457.3–456.96 mbsf) that is clearly delineated by a 40% decrease in carbonate content and 2–3‰ negative excursions in bulk carbonate δ^{13}C and δ^{18}O values (Fig. 2). The Benthic Foraminiferal Extinction Event (BFEE) is identified directly below the PETM at 457.3 mbsf based on the highest occurrences of the *Stensioina beccariformis*, *Gyroidinoides globosus* and *G. subangulatus*. The planktic foraminiferal genus *Morozovella* has its lowest occurrence at the base of the PETM and greatest diversity within the PETM. *Morozovella aequa* and *M. velascoensis* are restricted to the PETM. The latter species has rarely been found outside the PETM in the SW Pacific but *M. aequa* ranges into the middle late Eocene in New Zealand sections (Hornibrook et al. 1989). For nannofossils, taxa typical of the PETM in other regions, such as the *Rhomboaster* lineage, *Discoaster araneus* and *D. anartios* (e.g., Bybell and Self-Trail, 1994; Kahn and Aubry, 2004), are absent here. Instead, the nannofossil assemblage is characterized by deformed *Discoaster* specimens, many similar to *Discoaster nobilis* (e.g., Raffi and De Bernardi, 2008), as well as increased abundance of *Coccolithus* spp. and the presence of *Fasciculithus* spp. and *Bomolithus supremus*, which is restricted to the PETM interval at this site. Immediately above the PETM (456.92 mbsf), the abundances of *Fasciculithus* spp. and *Coccolithus* spp. decrease significantly, with a concomitant increase in *Zygrhablithus bijugatus*. As discussed below, the stable isotope record through the P-E transition indicates that the PETM is truncated, with only the onset and body of the CIE represented by these 34 cm of sediment.

An age-depth plot (Fig. S3) based on calcareous nannofossil and foraminiferal bioevents (Table S7) provides a preliminary guide to compacted sedimentation rates. This rate appears to have been relatively low in the Paleocene (0.4 to 0.45 cm/kyr) either side of the hiatus at ~463.4 mbsf, but approximately four times higher in the early Eocene (1.68 cm/kyr). However, a rather patchy distribution of events and uncertainty over the duration of hiatuses means that it is possible to construct an alternative age model in which rates were consistent across the Paleocene-Eocene transition (dashed line in Fig. S3). Although this implies that the sedimentation rate for the PETM interval could lie anywhere between the low Paleocene rate and the high Eocene rate, the lower rate is consistent with the duration of the CIE from onset to δ^{13}C minimum, i.e., ~45-66 kyrs (Röhl et al., 2007).

The base of the PETM coincides with a distinct colour change to a darker greenish-grey chalk that grades back into greenish-white chalk over 15 cm (Fig. 5). This dark interval is also highly burrowed. Burrowing is also evident in other parts of the core but it is less obvious in more pale lithologies. XRF core scanning shows an increase in Fe content at the base of this interval, followed by a cyclical decrease to background levels at 456.95 m (Fig. 5A). A lower resolution record of magnetic susceptibility in discrete samples reveals a similar trend: a peak near the base of the darker interval, followed by a quasi-cyclical decrease to background levels. The peaks are inferred to represent intervals of higher clay content based on the parallel trends in Fe and magnetic susceptibility. Many of the other peaks and troughs in the Fe record below and above the PETM are scanning artefacts related to core breaks. However, parallel peaks in magnetic susceptibility and Fe content in the lower part of core 45 (~457.7 mbsf) appears to be a robust signal although the cause is unknown. There are no accompanying changes in isotopic signature or obvious lithological changes at this level.

A 10 cm interval directly below the PETM also has a reduced carbonate concentration but there is no change in δ^{13}C (Fig. 2, 5B). As there is no accompanying increase in magnetic susceptibility or Fe content (Fig. 5A), the decrease in carbonate content seems to be due to an increase in silica, perhaps associated with the slight cooling indicated by a small positive shift in δ^{18}O of ~0.4‰ in both bulk and foraminiferal calcite (Fig. 2, 5D). Although the silica is presumed to be biogenic, siliceous microfossils have not been recovered from this interval.

For a sedimentation rate of 0.45 cm/kyr, the 34 cm thick PETM interval represents ~76 kyrs and the three peaks in Fe content represent a periodicity close to the precession band (~21 kyrs). Indeed, there is good agreement between the Fe cycles and δ^{13}C record at Site 277 and ODP Site 690 (Röhl et al., 2007), where the negative CIE occurs over three steps and the δ^{13}C minimum (Horizon C of Zachos et al., 2005) occurs within the third Fe peak. Based on this correlation with Site 690, we infer that the interval from the CIE onset to the base of Cycle 4 is preserved at Site 277, or the first 66 kyrs of the PETM (Röhl et al., 2007), implying a slight increase in sedimentation rate through the PETM (52 cm/kyr).

3.2. Stable isotopes

Bulk carbonate stable isotopes display a significant offset between δ^{18}O and δ^{13}C minima, with the δ^{18}O minimum occurring at the base and the δ^{13}C minimum in the upper part of the PETM (Fig. 2, 5B). The negative CIE of ~2‰ is slightly smaller than the average for marine sections (2.7‰; McInerney and Wing, 2011) and occurs gradually over the lower 20 cm of the PETM. In contrast, the 3‰ negative δ^{18}O excursion (OIE) is abrupt at the base of the PETM and is larger in magnitude than is known elsewhere (e.g., Bains et al. 1999; Dunkley Jones et al., 2013). If this a primary feature and due solely to a change in temperature, this excursion would equate to ~12°C of warming (Fig. 5D); however, it is most likely an artefact of diagenesis as is discussed below.

Examination of foraminiferal δ^{18}O and Mg/Ca ratios help to separate the diagenetic effects from the paleotemperature record. As none of the foraminifera recovered in this study have “glassy” preservation (Sexton et al. 2006; Pearson and Burgess, 2008; Kozdon et al., 2013), all are assumed to have been altered to varying degrees. We selected the best preserved specimens for isotopic analysis (Fig. 2, 5B, 6). Our results indicate that normal surface to deep δ^{13}C gradients are preserved in the foraminiferal tests, with bulk carbonate δ^{13}C values lying within the range of, or slightly lighter than, planktic foraminiferal δ^{13}C throughout the studied interval. An exception is noted in the basal PETM where two values are more positive than planktic δ^{13}C (Fig. 5B, 6B). Benthic δ^{13}C values are >0.7‰ lighter than both planktic and bulk carbonate values, apart from the basal PETM sample where a negative gradient of -0.37‰ occurs between *Acarinina* and *Cibicides* (Fig. 5B, 6B). The implication is that the onset of the CIE is recorded more strongly in planktic foraminifera (i.e. surface water CIE of -1.85‰) than in either benthic foraminifera (deep water CIE of -0.55‰) or bulk carbonate (CIE of -0.34‰ across equivalent sample interval).

If it were not for the large magnitude of the OIE across the same sample interval (-1.42‰, and -2.82‰ for the full OIE), we might argue for mixing across the boundary dampening the bulk carbonate CIE. However, the marked differences in the pattern of onset for the CIE and OIE suggest that there was no mixing of sediment across the boundary. Similarly, there is little evidence for the isotope record being affected by carbonate dissolution or burn-down (Dickens, 2000; Kozdon et al, 2013) below the base of the PETM. A weak positive shift in pre-PETM δ^{18}O values and reduced carbonate content appears to reflect cooler conditions as the shift is accompanied by a cooling trend in the benthic Mg/Ca ratio (Fig. 5D-E).

A similar offset between bulk and planktic δ^{13}C in the basal PETM was described for ODP Site 690, where Stoll (2005) showed close agreement between trends in stable isotopes for bulk carbonate, coccolith fractions and *Subbotina* but significant offsets with *Acarinina*, the latter recording an earlier CIE onset and a later OIE minimum. Stoll (2005) considered several possible causes for this offset and favoured differences in habitat and seasonal production. For Site 690, the correspondence between coccoliths and *Subbotina* suggests that coccolith production may have occurred at a lower level within the photic zone than the level preferred by *Acarinina*. For Site 277, the δ^{13}C gradient suggests a similar explanation but a different relationship. During the PETM onset, coccolith production appears to have occurred at a shallower level than that preferred by planktic foraminifera at this site. This may also explain why bulk carbonate δ^{18}O is more depleted than planktic values in this interval, i.e. coccolith production in shallower and warmer waters. Given that this relationship is only fully expressed at the PETM onset, we suggest that this might have been a time of increased stratification and differentiation between water masses in the upper water column at this site. Nunes and Norris (2006) used ageing gradients in benthic δ^{13}C to infer a switch in deep water formation across the P/E boundary from the Southern Ocean to the Northern Hemisphere. Our benthic δ^{13}C data from Site 277 support this hypothesis. Site 277 benthic d13C is 0.46‰ higher than values in the equatorial Pacific prior to the PETM but 0.12‰ lower within the PETM. It seems likely that comparable changes occurred in surface water circulation.

With the CIE onset seeming explicable in terms of relationships between coccolith and foraminiferal niches and changes in ocean circulation, we turn our attention to the stepped decline in the bulk carbonate CIE at Site 277. Stoll (2005) argued that a similar series of three steps in the bulk carbonate CIE seen at Site 690 reflect the greater capacity for coccoliths to record changes in ocean conditions at a finer scale than is possible from the less abundant foraminiferal fraction. Although we lack the resolution in the foraminiferal record to compare sites 277 and 690 in detail, we observe the same trend and note a broad correlation with the three Fe peaks. It seems likely that these steps represent precessional modulation of the release of ^{13}C-depleted carbon into the ocean over ~60 kyrs (Röhl et al., 2007; Sluijs et al., 2007).

3.3 Diagenetic modification of δ^{18}O values

As noted above, the bulk carbonate δ^{18}O values at Site 277 intergrade between benthic and planktic foraminiferal values in the Paleocene and in the Eocene interval above the PETM (Fig. 6A, 6C). Moreover, several planktic foraminiferal δ^{18}O values are only ~0.3‰ lighter than benthic values in the Paleocene (Fig. 2, 6C). Conversely, all bulk carbonate δ^{18}O values lie within the range of planktic foraminiferal δ^{18}O within the PETM (Fig. 6B) and, indeed, bulk carbonate δ^{18}O is lighter than planktic foraminiferal δ^{18}O in the basal PETM (Fig. 2, 5D). We contend that diagenetic effects explain these relationships. The bulk carbonate δ^{18}O has been shifted toward heavier values during early diagenesis (at seafloor temperature) over much of the section above and below the CIE (Schrag et al., 1995; Sexton et al., 1996; Kozdon et al, 2013), whereas within the PETM interval the bulk and foraminiferal carbonate appears to have undergone less diagenetic alteration. We suggest that the increase in clay in the PETM protected coccoliths and foraminifera from wholesale recrystallization, preserving more of the original δ^{18}O signal. The presence of clay serves to reduce sediment porosity and retard carbonate recrystallization (Sexton et al., 2006). This explains the large magnitude of the bulk carbonate δ^{18}O excursion across the P-E boundary, with the δ^{18}O values below the excursion having been altered toward heavier values (Fig. 2, 5D-E).

The planktic foraminiferal δ^{18}O values at Site 277 appear to be compromised to varying degrees by seafloor diagenesis throughout the interval studies. The surface-to-deep temperature gradient may be expected to be reduced in high latitude regions such as the Campbell Plateau. Mean annual Subantarctic Water is ~6° warmer than Antarctic Intermediate Water in the present-day Southern Ocean (Carter et al., 1999). However, the very low planktic-benthic δ^{18}O gradient in the Paleocene and post-PETM Eocene (0.8‰, 3°C) suggests alteration of planktic δ^{18}O toward benthic values (Fig. 2, 5D, 6C). The gradient is only slightly higher in the PETM (1.1‰, 4°C), suggesting that a cool bias affects all paleotemperatures derived from planktic δ^{18}O through the P-E transition at this site. The degree of this bias is uncertain. The warmer paleotemperature derived from Mg/Ca ratios may be more reliable but, as is discussed below, diagenesis may result in a warm bias.

3.4. Diagenetic modification of Mg/Ca ratios

There is evidence that diagenesis also has significant and specific effects on Mg/Ca values (Oomori et al., 1987; Kozdon et al., 2013). As noted earlier, we observe a distinct relationship between the Mg/Ca ratio and the geochemical proxy for diagenesis, the Sr/Ca ratio, once we have screened for silicate contamination (Fig. 3). For *Cibicides*, the full screened dataset shows a roughly horizontal trend, with little change in Sr/Ca as Mg/Ca varies. This suggests that this genus is relatively immune to the effects of diagenesis, perhaps related to its relatively thick and smooth wall. However, if we consider Paleocene and PETM samples separately, we observe that Paleocene analyses tend to have lower Sr/Ca ratios than PETM samples and exhibit a weak trend in which Mg/Ca increases as Sr/Ca decreases. This general relationship has also been identified by Kozdon et al. (2013) as a guide to diagenetic alteration, albeit the impact on Mg/Ca ratios is an order of magnitude smaller than found in laboratory experiments (Oomori et al., 1987). The trend is more obvious in *Acarinina* at Site 277, probably because the thinner-walled and more irregular test provides more surfaces for interaction with pore waters and hence facilitates diagenetic alteration. For the full data set, a significant negative correlation is observed, with Mg/Ca increasing as Sr/Ca decreases. A weaker trend is evident in the PETM data but a much stronger trend is shown by the Paleocene data. From these observations we can draw the following conclusions: (i) *Acarinina* is more prone to diagenesis than *Cibicides*, (ii) diagenesis is greater in the Paleocene than in the PETM, and (iii) diagenesis causes an increase in the Mg/Ca ratio and implies that paleotemperatures may be overestimated for some taxa, such as *Acarinina*, and in some intervals such as the Paleocene at this site. This may explain why the SST estimates for the Paleocene based on *Acarinina* Mg/Ca ratios are higher than expected (Fig. 5D, E).

3.5. Paleotemperature

Taking into account these numerous complications, we can make some general observations on temperature changes through the P-E transition at Site 277. Estimates for SFT from benthic foraminiferal $\delta^{18}O$ and Mg/Ca are relatively consistent at 12–15°C for the late Paleocene (Fig. 5D), with coolest SFTs of 11−12°C occurring in the uppermost 10 cm of Paleocene where carbonate content is also lower than background. Benthic $\delta^{18}O$ and Mg/Ca values indicate SFT warmed by ~5−6°C across the P-E boundary, with SFTs of up to ~19°C in the basal PETM. There is little evidence for further warming of SFT in the body of the PETM. Following the PETM, SFT drops abruptly by ~5°C and remains stable at ~13°C in the overlying Eocene interval (Fig. 5D−E). Diagenesis may explain why some Paleocene Mg/Ca ratios yield higher SFTs than the benthic $\delta^{18}O$ values.

The SST record across the P-E boundary is much more difficult to interpret. The small offset between benthic and planktic $\delta^{18}O$ (~3°C) combined with the large offset between planktic $\delta^{18}O$ and

Mg/Ca values (~12°C) in the Paleocene, are likely consequences of diagenetic alteration, with the actual SST lying somewhere between 15 and 27°C (Fig. 5D). Similarly, the degree of warming across the PETM may be accentuated for δ^{18}O but effectively dampened for Mg/Ca due to the effects discussed above. For this reason, the observation that the relative SST increase is ~5−6°C for both proxies (Fig. 5E) is difficult to explain even though it is consistent with the SFT record. Diagenetic effects appear to decrease across the P-E boundary, based on our analysis of the benthic−planktic δ^{18}O gradient and the Sr/Ca ratio. Therefore, we would predict that the relative increase in SST across the boundary would be greater for planktic δ^{18}O than for Mg/Ca. It may be that the patchy nature of the record through this interval is masking these relationships. Irrespective of the true magnitude of SST change across the P-E boundary, planktic Mg/Ca ratios indicate warmest SSTs in the lower PETM, stable SSTs through the body of the PETM (albeit ~3°C cooler) and an abrupt ~4°C cooling directly above the PETM.

The 5-6°C increase in SST is similar to other PETM records. At ODP Site 1172, the TEX_{86} record indicates that SST increased by 6°C across the P/E boundary (Sluijs et al., 2011) and SST during the PETM was 3−4°C warmer than average Paleocene values (Fig. 7). Elsewhere, temperature anomalies within the PETM range from +4−5°C in low latitudes (Zachos et al., 2003; Aze et al., 2014) to +8°C in high latitudes (Thomas et al., 2002; Frieling et al., 2014) and some low latitude coastal sites (Zachos et al., 2006).

The peak SSTs of ~32° within the PETM are consistent with TEX_{86}-based SSTs from the PETM at ODP Site 1172 (Sluijs et al., 2011) and in the mid-Waipara section, eastern South Island, New Zealand (Hollis et al, 2012). At these locations, the two calibrations for TEX_{86} introduced by Kim et al. (2010) yield peak SSTs for the PETM of 32–34°C (TEX_{86}^{H}) or 26–28°C (TEX_{86}^{L}). Although the TEX_{86}^{L} calibration was considered more suitable for this region based on comparisons with other SST proxies (Hollis et al., 2012), a new Bayesian approach to TEX_{86} calibrations (Tierney and Tingley, 2014) yields temperatures for the PETM that are very similar to the TEX_{86}^{H} calibration. These PETM SSTs are also consistent with the SST estimates of 26°C that were derived from TEX_{86} and $U^{K'}_{37}$ for the late Eocene at Site 277 (Liu et al, 2009), given that deep sea temperatures cooled by ~8°C through the Eocene (Zachos et al., 2008).

There is considerable debate about the veracity of such high temperature estimates in high latitude regions, with concerns raised about calibrations, seasonal bias and archaeol physiology processes (Hollis et al., 2012; Taylor et al. 2013; Inglis et al., under revision.). However, the consistency between SSTs derived from Mg/Ca and TEX_{86} (Burgess et al., 2008; Hollis et al., 2012) suggests that the high temperatures are due to factors that the proxies may have in common, such as a warm-season bias, rather than problems with respective calibrations or physiological factors.

3.6. Comparison with other PETM records

A comparison of the PETM record at DSDP Site 277 with nearby records at Mead Stream (Hollis et al., 2005a; Nicolo et al., 2010) and ODP Site 1172 (Sluijs et al., 2011) reveals several significant features (Fig. 7). Firstly, there seems little doubt that only the onset of the CIE is preserved at Site 277. The pattern of decreasing $\delta^{13}C$ is very similar to the expanded onset at Mead Stream. As noted above, the stepped decrease in $\delta^{13}C$ is also observed at ODP Site 690 (Röhl et al., 2007). However, the pattern of warming at Site 277 is different from Site 1172. At Site 277, the most pronounced increase in temperatures occurs at the base of the PETM and is associated with a weak negative $\delta^{13}C$ excursion. Higher in the PETM, temperatures remain stable or decrease slightly as $\delta^{13}C$ decreases. At Site 1172, the TEX_{86} record indicates pronounced warming at the base of the PETM but SST continues to increase and peaks just above the $\delta^{13}C$ minimum. No direct measurements of temperature have been obtained from the indurated lithologies at Mead Stream. However, changes in radiolarian assemblages identify a definite peak in low-latitude species, also directly above the $\delta^{13}C$ minimum (red star in Fig. 7) (Hollis, 2006).

The implication of these differences between SW Pacific sites is that the primary warming pulse occurred in both intermediate and surface waters at the initiation of the PETM on the Campbell Plateau, whereas this initial event was only the precursor to progressive warming in the continental margin settings to the west and north (Fig. 1). A similar pattern of warming is evident in the Atlantic Ocean, where the $\delta^{18}O$ records for ODP sites 690 and 1051 suggest that peak warming occurred at the onset of the PETM in the southern Atlantic (Site 690) but at the same level as the CIE minimum in the western North Atlantic (Bains et al., 1999; Stoll, 2005). We cannot be sure that there was not a second warming pulse above the onset of the PETM on the Campbell Plateau because the main phase of the PETM does not appear to be preserved at Site 277. However, the absolute SST values at Site 277 are similar to the peak SSTs at Site 1172, i.e. 30−32°C. Therefore, we need to explain how the Campbell Plateau warmed at the start of the PETM and stayed warm through the onset, while the East Tasman Plateau warmed to a lesser extent initially but then continued to warm into the main phase of the PETM, with both sites experiencing at least seasonal SST maxima in excess of 30°C. We speculate that the gradual warming that followed Southern Ocean cooling at 59 Ma (Hollis et al., 2014) exceeded a threshold at the start of the PETM that caused the southward expansion of the subtropical-tropical gyre over the Campbell Plateau. This gyre was sustained through the PETM onset but resulted in no additional warming at this location. It is notable that several warm-water species of *Morozovella* are restricted to the PETM at Site 277. The influence of the gyre may have also reached the East Tasman Plateau but an additional factor continued to warm the region into the main phase of the PETM. This factor may have been a proto-Eastern Australian Current, intensifying its southwestern reach during times of extreme warming (e.g. Cortese et al., 2013).

4. Conclusions

Part of the motivation in undertaking this study and presenting these results is that there is interest in re-drilling this site as part of IODP Proposal 567 (Paleogene South Pacific APC Transect) using new technology that will greatly improve the quantity and quality of core recovery. We have shown that even with this improved recovery, extracting a paleoclimate record will still be complicated by diagenesis, recrystallization and hiatuses. In order to recover a more reliable climate proxy records for the Paleogene of this region, we recommend consideration of alternative or additional Campbell Plateau sites where sedimentation rates and clay input is predicted to have been higher than at Site 277 (Cook et al., 1999). Nevertheless, we have also illustrated how a multi-proxy approach can be used to extract a climate history from this complicated record with due consideration of the effects of differential diagenesis, both between taxonomic groups and across stratigraphic horizons.

The onset of the PETM is recorded in a 34 cm thick interval within core 45 at DSDP Site 277. A significant and rapid warming of surface and deep waters at the onset of the PETM at Site 277 parallels a pronounced decline in carbonate concentration and a modest initial negative $\delta^{13}C$ excursion of ~1‰. The full extent of the 2‰ negative $\delta^{13}C$ excursion occurred gradually over an interval in which temperatures remained stable or declined slightly. Therefore, it would seem that an initial carbon perturbation had a pronounced effect on southern Pacific Ocean circulation, causing poleward expansion of warm surface and intermediate waters. In contrast, the full expression of the event had little additional effect, perhaps because a threshold was exceeded at the initial event.

Supplementary material related to this article is available online at: ....

Acknowledgements. This research relied on archival DSDP samples and data provided by the International Ocean Discovery Program (IODP) and was funded by the New Zealand Government through the GNS Science Global Change through Time Programme (540GCT12, 540GCT62). We thank Paul Pearson and Reinhard Kozdon for very constructive reviews, Appy Sluijs for editorial handling, and Randall McDonnell (GNS Science) for technical support.

References

Anand, P., Elderfield, H., Conte, M.H., 2003. Calibration of Mg/Ca thermometry in planktonic foraminifera from a sediment trap time series. Paleoceanography 18 (2), 1050, doi: 10.1029/2002pa000846

Aubry, M.-P., Ouda, K., Dupuis, C., Berggren, W.A. and Van Couvering, J.A., 2007. The Global Standard Stratotype-section and Point (GSSP) for the base of the Eocene Series in the Dababiya section (Egypt). Episodes 30, 271-286.

Aze, T., Pearson, P.N., Dickson, A.J., Badger, M.P.S., Bown, P.R., Pancost, R.D., Gibbs, S.J., Huber, B.T., Leng, M.J., Coe, A.L., Cohen, A.S., Foster, G.L., 2014. Extreme warming of tropical waters during the Paleocene–Eocene Thermal Maximum. Geology 42, 739-742.

Bains, S., Corfield, R.M. and Norris, R.D., 1999. Mechanisms of climate warming at the end of the Paleocene. Science 285, 724-727.

Barker, S., Greaves, M., Elderfield, H., 2003. A study of cleaning procedures used for foraminiferal Mg/Ca paleothermometry. Geochemistry, Geophysics, Geosystems 4, 8407, doi:8410.1016/j.quascirev.2004.8407.8016.

Beerling, D.J., Royer, D.L., 2011. Convergent Cenozoic CO2 history. Nature Geoscience 4, 418-420.

Bown, P.R. (Ed.), 1998. Calcareous Nannofossil Biostratigraphy. Kluwer Academie, London, 315p.

Bown, P.R., Young, J.R., 1998. Techniques. In: Bown, P.R. (Ed.), Calcareous Nannofossil Biostratigraphy. Kluwer Academie, London, 16–28.

Burgess, C.E., Pearson, P.N., Lear, C.H., Morgans, H.E.G., Handley, L., Pancost, R.D., Schouten, S., 2008. Middle Eocene climate cyclicity in the southern Pacific: Implications for global ice volume. Geology 36, 651-654.

Bybell, L.M., Self-Trail, J., M, 1994. Evolutionary, biostratigraphic, and taxonomic study of calcareous nannofossils from a continuous Paleocene-Eocene boundary section in New Jersey. US Geological Survey Professional Paper 1554, 114 p.

Carter, R.M., McCave, I.N., Richter, C. et al., 1999. Proceedings of the Ocean Drilling Program, initial reports, volume 181: Southwest Pacific gateways, Sites 1119-1125.

Coggon, R.M., Teagle, D.A.H., Smith-Duque, C.E., Alt, J.C., Cooper, M.J., 2010. Reconstructing Past Seawater Mg/Ca and Sr/Ca from Mid-Ocean Ridge Flank Calcium Carbonate Veins. Science 327, 1114-1117.

Cook, R.A., Sutherland, R. and Zhu, H. (1999) Cretaceous−Cenozoic geology and petroleum systems of the Great South Basin, New Zealand. Institute of Geological & Nuclear Sciences Monograph 20. Institute of Geological and Nuclear Sciences, Lower Hutt, 190 pp.

Cooper, R.A., 2004. The New Zealand Geological Timescale. Institute of Geological and Nuclear Sciences Monograph 22. Institute of Geological and Nuclear Sciences, Lower Hutt, 284 pp.

Cortese, G., Dunbar, G.B., Carter, L., Scott, G., Bostock, H., Bowen, M., Crundwell, M., Hayward, B.W., Howard, W., Martinez, J.I., Moy, A., Neil, H., Sabaa, A. and Sturm, A., 2013. Southwest Pacific Ocean response to a warmer world: insights from Marine Isotope Stage 5e. Paleoceanography 28, 1–14, doi:10.1002/palo.20052.

Cramer, B.S., Miller, K.G., Barrett, P.J., Wright, J.D., 2011. Late Cretaceous-Neogene trends in deep ocean temperature and continental ice volume: Reconciling records of benthic foraminiferal geochemistry (□^{18}O and Mg/Ca) with sea level history. Journal of Geophysical Research - Oceans 116, C12023.

Creech, J.B., Baker, J.A., Hollis, C.J., Morgans, H.E.G., Smith, E.G.C., 2010. Eocene sea temperatures for the mid-latitude southwest Pacific from Mg/Ca ratios in planktonic and benthic foraminifera. Earth and planetary science letters 299(3/4), 483-495; doi:410.1016/j.epsl.2010.1009.1039.

Crouch, E.M., Heilmann-Clausen, C., Brinkhuis, H., Morgans, H.E.G., Egger, H., Schmitz, B., 2001. Global dinoflagellate event associated with the late Paleocene thermal maximum. Geology 29, 315-318.

Crouch, E.M., Dickens, G.R., Brinkhuis, H., Aubry, M.P., Hollis, C.J., Rogers, K.M., Visscher, H., 2003. The *Apectodinium* acme and terrestrial discharge during the Paleocene-Eocene thermal maximum : new palynological, geochemical and calcareous nannoplankton observations at Tawanui, New Zealand. Palaeogeography, palaeoclimatology, palaeoecology 194(4), 387-403.

Dickens, G.R., 2003. Rethinking the global carbon cycle with a large, dynamic and microbially mediated gas hydrate capacitor. Earth and Planetary Science Letters 213, 169-183.

Dickens, G.R., 2011. Down the Rabbit Hole: toward appropriate discussion of methane release from gas hydrate systems during the Paleocene-Eocene thermal maximum and other past hyperthermal events. Clim. Past 7, 831-846.

Dickens, G.R., Castillo, M.M., Walker, J.C.G., 1997. A blast of gas in the latest Paleocene: Simulating first-order effects of massive dissociation of oceanic methane hydrate. Geology 25, 259-262.

Dickens, G.R., O'Neil, J.R., Rea, D.K., Owen, R.M., 1995. Dissociation of oceanic methane hydrate as a cause of the carbon isotope excursion at the end of the Paleocene. Paleoceanography 10, 965-972.

Dunkley Jones, T., Lunt, D.J., Schmidt, D.N., Ridgwell, A., Sluijs, A., Valdes, P.J., and Maslin, M., 2013. Climate model and proxy data constraints on ocean warming across the Paleocene–Eocene Thermal Maximum, Earth Sci. Rev., 125, 123-145, doi: 10.1016/j.earscirev.2013.07.004.

Eggins, S., De Deckker, P., Marshall, J., 2003. Mg/Ca variation in planktonic foraminifera tests: implications for reconstructing palaeo-seawater temperature and habitat migration. Earth and Planetary Science Letters 212, 291-306, doi:210.1016/S0012-1821X(1003)00283-00288.

Evans, D., Müller, W., 2012. Deep time foraminifera Mg/Ca paleothermometry: Nonlinear correction for secular change in seawater Mg/Ca. Paleoceanography 27, PA4205.

Frieling, J., Iakovleva, A.I., Reichart, G.-J., Aleksandrova, G.N., Gnibidenko, Z.N., Schouten, S., Sluijs, A., 2014. Paleocene–Eocene warming and biotic response in the epicontinental West Siberian Sea. Geology 42, 767-770.

Gradstein, F.M., Ogg, J.G., Schmitz, M., Ogg, G., 2012. The Geologic Time Scale 2012. Elsevier Science BV, Oxford, UK.

Greaves, M., Barker, S., Daunt, C., Elderfield, H., 2005. Accuracy, standardization, and interlaboratory calibration standards for foraminiferal Mg/Ca thermometry. Geochemistry, Geophysics, Geosystems 6, doi:10.1029/2004GC000790.

Hancock, H.J.L., Dickens, G.R., Strong, C.P., Hollis, C.J., Field, B.D., 2003. Foraminiferal and carbon isotope stratigraphy through the Paleocene-Eocene transition at Dee Stream, Marlborough, New Zealand. New Zealand Journal of Geology and Geophysics 46, 1-19.

Handley, L., Crouch, E.M., Pancost, R.D., 2011. A New Zealand record of sea level rise and environmental change during the Paleocene-Eocene Thermal Maximum. Palaeogeography, Palaeoclimatology, Palaeoecology 305, 185-200.

Hasiuk, F.J., Lohmann, K.C., 2010. Application of calcite Mg partitioning functions to the reconstruction of paleocean Mg/Ca. Geochimica et Cosmochimica Acta 74, 6751-6763.

Higgins, J.A., Schrag, D.P., 2006. Beyond methane: Towards a theory for the Paleocene-Eocene Thermal Maximum. Earth and Planetary Science Letters 245, 523-537.

Hollis, C.J., 2006. Radiolarian faunal change across the Paleocene-Eocene boundary at Mead Stream, New Zealand. Eclogae Geologicae Helvetiae 99, S79-S99.

Hollis, C.J., Dickens, G.R., Field, B.D., Jones, C.J., Strong, C.P., 2005a. The Paleocene-Eocene transition at Mead Stream, New Zealand: a southern Pacific record of early Cenozoic global change. Palaeogeography, Palaeoclimatology, Palaeoecology 215, 313-343.

Hollis, C.J., Field, B.D., Jones, C.M., Strong, C.P., Wilson, G.J., Dickens, G.R., 2005b. Biostratigraphy and carbon isotope stratigraphy of uppermost Cretaceous-lower Cenozoic in middle Clarence valley, New Zealand. Journal of the Royal Society of New Zealand 35, 345-383.

Hollis, C.J., Taylor, K.W.T., Handley, L., Pancost, R.D., Huber, M., Creech, J., Hines, B., Crouch, E.M., Morgans, H.E.G., Crampton, J.S., Gibbs, S., Pearson, P., Zachos, J.C., 2012. Early Paleogene temperature history of the Southwest Pacific Ocean: reconciling proxies and models. Earth and Planetary Science Letters 349-350, 53-66.

Hollis, C.J., Waghorn, D.B., Strong, C.P., Crouch, E.M., 1997. Integrated Paleogene biostratigraphy of DSDP site 277 (Leg 29): foraminifera, calcareous nannofossils, Radiolaria, and palynomorphs. Institute of Geological & Nuclear Sciences science report 97/7, 1-73.

Hollis, C.J., Tayler, M.J.S., Andrew, B., Taylor, K.W., Lurcock, P., Bijl, P.K., Kulhanek, D.K., Crouch, E.M., Nelson, C.S., Pancost, R.D., Huber, M., Wilson, G.S., Ventura, G.T., Crampton, J.S., Schiøler, P., Phillips, A., 2014. Organic-rich sedimentation in the South Pacific Ocean associated with Late Paleocene climatic cooling. Earth-Science Reviews 134, 81-97.

Horita, J., Zimmermann, H., Holland, H.D., 2002. Chemical evolution of seawater during the Phanerozoic: Implications from the record of marine evaporites. Geochimica et Cosmochimica Acta 66, 3733-3756.

Hornibrook, N.de B., 1992. New Zealand Cenozoic marine paleoclimates : a review based on the distribution of some shallow water and terrestrial biota, in: Tsuchi, R., Ingle, J.C. (Eds.), Pacific Neogene: environment, evolution and events. University of Tokyo Press, Tokyo, pp. 83-106.

Hornibrook, N.deB., Brazier, R.C., Strong, C.P., 1989. Manual of New Zealand Permian to Pleistocene foraminiferal biostratigraphy. New Zealand Geological Survey Paleontological Bulletin 56, 175 p.

Inglis, G.N., Farnsworth, A., Lunt, D., Foster, G.L., Hollis, C.J., Pagani, M., Jardine, P.E., Pearson, P.N., Markwick, P., Raynman, L., Galsworthy, A.M.J., Pancost, R.D., in review. Descent towards the Icehouse: Eocene sea surface cooling inferred from GDGT distributions. Paleoceanography.

Jones, G.A., Kaiteris, P., 1983. A vacuum-gasometric technique for rapid and precise analysis of calcium carbonate in sediment and soils. Journal of Sedimentary Petrology 53, 655-660.

Joughin, I., Smith, B.E., Medley, B., 2014. Marine Ice Sheet Collapse Potentially Under Way for the Thwaites Glacier Basin, West Antarctica. Science 344, 735-738.

Kahn, A., Aubry, M.-P., 2004. Provincialism associated with the Paleocene/Eocene thermal maximum: temporal constraint. Marine Micropaleontology 52, 117-131.

Kaiho, K., Arinobu, T., Ishiwatari, R., Morgans, H.E.G., Okada, H., Takeda, N., Tazaki, K., Zhou, G., Kajiwara, Y., Matsumoto, R., Hirai, A., Niitsuma, N., Wada, H., 1996. Latest Paleocene benthic foraminiferal extinction and environmental changes at Tawanui, New Zealand. Paleoceanography 11, 447-465.

Katz, M.E., Katz, D.R., Wright, J.D., Miller, K.G., Pak, D.K., Shackleton, N.J. and Thomas, E., 2003. Early Cenozoic benthic foraminiferal isotopes: Species reliability and interspecies correction factors. Paleoceanography 18 (2), 1024, doi: 10.1029/2002PA000798.

Kennett, J.P., 1975. Initial reports of the Deep Sea Drilling Project, volume 29. US Govt Printing Office, Washington.

Kennett, J.P., 1977. Cenozoic evolution of Antarctic glaciation, the Circum-Antarctic Ocean, and their impact on global paleoceanography. Journal of Geophysical Research 82, 3843-3860.

Kennett, J.P., 1980. Paleoceanographic and biogeographic evolution of the Southern Ocean during the Cenozoic, and Cenozoic microfossil datums. Palaeogeography, Palaeoclimatology, Palaeoecology 31, 123-152.

Kent, D.V., Cramer, B.S., Lanci, L., Wang, D., Wright, J.D., Van der Voo, R., 2003. A case for a comet impact trigger for the Paleocene/Eocene thermal maximum and carbon isotope excursion. Earth and Planetary Science Letters 211, 13-26.

Kim, S.-T., O'Neil, J.R., 1997. Equilibrium and nonequilibrium oxygen isotope effects in synthetic carbonates. Geochimica et Cosmochimica Acta 61, 3461-3475.

Kim, J.-H., van der Meer, J., Schouten, S., Helmke, P., Willmott, V., Sangiorgi, F., Koç, N., Hopmans, E.C., Damsté, J.S.S., 2010. New indices and calibrations derived from the distribution of crenarchaeal isoprenoid tetraether lipids: Implications for past sea surface temperature reconstructions. Geochimica et Cosmochimica Acta 74, 4639-4654.

Kozdon, R., Kelly, D.C., Kitajima, K., Strickland, A., Fournelle, J.H. and Valley, J.W., 2013. In situ $\delta^{18}O$ and Mg/Ca analyses of diagenetic and planktic foraminiferal calcite preserved in a deep-sea record of the Paleocene-Eocene thermal maximum. Paleoceanography 28, 517-528.

Lear, C.H., Rosenthal, Y., Slowey, N., 2002. Benthic foraminiferal Mg/Ca-paleothermometry: a revised core-top calibration. Geochimica et Cosmochimica Acta 66, 3375-3387.

Liu, Z., Pagani, M., Zinniker, D., DeConto, R., Huber, M., Brinkhuis, H., Shah, S.R., Leckie, R.M., Pearson, A., 2009. Global Cooling During the Eocene-Oligocene Climate Transition. Science 323, 1187-1190.

Martini, E., 1970. Standard Paleogene calcareous nannoplankton zonation. Nature 226, 560–561.

Martini, E., 1971. Standard Tertiary and Quaternary calcareous nannoplankton zonation. In: Farinacci, A. (Ed.), Proceedings of the Planktonic Conference II, Roma, 1970. Edizioni Tecnoscienze, Rome, 739–785.

McInerney, F.A., Wing, S.L., 2011. The Paleocene-Eocene Thermal Maximum: A Perturbation of Carbon Cycle, Climate, and Biosphere with Implications for the Future. Annual Review of Earth and Planetary Sciences 39, 489-516.

Nelson, C.S., Cooke, P.J., 2001. History of oceanic front development in the New Zealand sector of the Southern Ocean during the Cenozoic: a synthesis. New Zealand journal of geology and geophysics 44(4), 535-553.

Nicolo, M.J., Dickens, G.R., Hollis, C.J., Zachos, J.C., 2007. Multiple early Eocene hyperthermals : their sedimentary expression on the New Zealand continental margin and in the deep sea. Geology 35(8), 699-702; doi:610.1130/G23648A.23641.

Nicolo, M.J., Dickens, G.R., Hollis, C.J., 2010. South Pacific intermediate water oxygen depletion at the onset of the Paleocene-Eocene thermal maximum as depicted in New Zealand margin sections. Paleoceanography 25, PA4210, doi:4210.1029/2009PA001904.

Norris, R.D., Wilson, P.A., Blum, P., and Expedition 342 Scientists, 2014. Proceedings of the IODP. 342, doi:10.2204/iodp.proc.2342.2014.

Nunes, F. and Norris, R.D. , 2006. Abrupt reversal in ocean overturning during the Palaeocene/Eocene warm period. Nature (London) 439, 60-63.

Olsson, R.K., Hemleben, C., Berggren, W.A., Huber, B.T., 1999. Atlas of Paleocene planktonic Foraminifera. Smithsonian Contributions to Paleobiology 85, 252 p.

Oomori, T., H. Kaneshima, Y. Maezato, and Y. Kitano, 1987. Distribution coefficient of Mg^{2+} ions between calcite and solution at 10–50°C, Marine Chemistry, 20, 327–336.

Pearson, P.N. and Burgess, C.E., 2008. Foraminifer test preservation and diagenesis: comparison of high latitude Eocene sites, Geological Society, London, Special Publications 303(1), 59-72.

Pearson, P.N., Olsson, R.K., Huber, B.T., Hemleben, C., Berggren, W.A., 2006. Atlas of Eocene Planktonic Foraminifera, Cushman Foundation Special Publication no. 41, 514 p.

Pearson, P.N., van Dongen, B.E., Nicholas, C.J., Pancost, R.D., Schouten, S., Singano, J.M., Wade, B.S., 2007. Stable warm tropical climate through the Eocene Epoch. Geology 35, 211-214.

Perch-Nielsen, K., 1985. Cenozoic calcareous nannofossils. In: Bolli, H.M., Saunders, J.B., and Perch-Nielsen, K. (Eds.), Plankton Stratigraphy. Cambridge University Press, Cambridge, 427–554.

Quillévéré, F., Norris, R.D., 2003. Ecological development of acarininids (planktonic foraminifera) and hydrographic evolution of Paleocene surface waters. GSA Special Papers 369, 223-238.

Raine, J.I., Beu, A.G., Boyes, A.F., Campbell, H.J., Cooper, R.A., Crampton, J.S., Crundwell, M.P., Hollis, C.J., Morgans, H.E.G., 2015. Revised calibration of the New Zealand Geological Timescale: NZGT2015/1. GNS Science Report 2012/39, 1-53.

Raffi, I., De Bernardi, B., 2008. Response of calcareous nannofossils to the Paleocene–Eocene Thermal Maximum: Observations on composition, preservation and calcification in sediments from ODP Site 1263 (Walvis Ridge—SW Atlantic). Marine Micropaleontology 69, 119-138.

Rampino, M.R., 2013. Peraluminous igneous rocks as an indicator of thermogenic methane release from the North Atlantic Volcanic Province at the time of the Paleocene–Eocene Thermal Maximum (PETM). Bulletin of Volcanology 75, 1-5.

Richter, T.O., van der Gaast, S., Kaster, B., Vaars, A., Gieles, R., de Stigter, H.C., De Haas, H., van Weering, T.C.E., 2006. The Avaatech XRF core scanner: technical description and applications to NE Atlantic sediments. Geological Society of London, Special Publications 267, 39–50. doi:10.1144/GSL.SP.2006.267.01.03

Röhl, U., Westerhold, T., Bralower, T.J. and Zachos, J.C., 2007. On the duration of the Paleocene-Eocene thermal maximum (PETM). Geochemistry, Geophysics, Geosystems 8, doi: 10.1029/2007GC001784

Schmidt, G.A., Annan, J.D., Bartlein, P.J., Cook, B.I., Guilyardi, E., Hargreaves, J.C., Harrison, S.P., Kageyama, M., LeGrande, A.N., Konecky, B., Lovejoy, S., Mann, M.E., Masson-Delmotte, V., Risi, C., Thompson, D., Timmermann, A., Tremblay, L.B., and Yiou, P., 2014. Using palaeo-climate comparisons to constrain future projections in CMIP5, Clim. Past 10, 221-250, doi: 10.5194/cp-10-221-2014.

Schrag, D.P., 1999. Effect of diagenesis on the isotopic record of late Paleogene tropical sea surface temperatures. Chemical Geology 161, 215-224.

Schrag, D.P., DePaolo, D.J., Richter, F.M., 1995. Reconstructing past sea surface temperatures: Correcting for diagenesis of bulk marine carbonate. Geochimica et Cosmochimica Acta 59, 2265-2278.

Schweizer, M., Pawlowski, J., Kouwenhoven, T. and van der Zwaan, B., 2009. Molecular phylogeny of common cibicidids and related Rotaliida (Foraminifera) based on small subunit rDNA sequences. The Journal of Foraminiferal Research 39, 300-315.

Sexton, P.F., Wilson, P.A., Pearson, P.N., 2006. Microstructural and geochemical perspectives on planktic foraminiferal preservation: ‘‘Glassy’’ versus ‘‘Frosty’’. Geochemistry, Geophysics, Geosystems - G^3 7, doi: 10.1029/2006GC001291.

Shackleton, N.J., Kennett, J.P., 1975. Paleotemperature history of the Cenozoic and the initiation of Antarctic glaciation : oxygen and carbon isotope analyses in DSDP sites 277, 279, and 281. Initial reports of the Deep Sea Drilling Project 29, 743-755.

Slotnick, B.S., Dickens, G.R., Nicolo, M., Hollis, C.J., Crampton, J.S., Zachos, J.C., Sluijs, A., 2012. Numerous large amplitude variations in carbon cycling and terrestrial weathering throughout the latest Paleocene and earliest Eocene. Journal of Geology 120, 487-505.

Sluijs, A., Bowen, G., Brinkhuis, H., Lourens, L., Thomas, E., 2007. The Palaeocene-Eocene Thermal Maximum super greenhouse: biotic and geochemical signatures, age models and mechanisms of global change, in: Willliams, M. et al. (Eds.), Deep time perspectives on climate change: marrying the signal from computer models and biological proxies. The Geological Society of London, Special Publication, pp. 323-347.

Sluijs, A., Bijl, P.K., Schouten, S., Roehl, U., Reichart, G.J., Brinkhuis, H., 2011. Southern ocean warming, sea level and hydrological change during the Paleocene-Eocene thermal maximum. Clim. Past 7, 47-61.

Stanley, S.M., Hardie, L.A., 1998. Secular oscillations in the carbonate mineralogy of reef-building and sediment-producing organisms driven by tectonically forced shifts in seawater chemistry. Palaeogeography, Palaeoclimatology, Palaeoecology 144, 3-19.

Stoll, H.M., 2005. Limited range of interspecific vital effects in coccolith stable isotopic records during the Paleocene-Eocene thermal maximum. Paleoceanography 20, doi: 10.1029/2004PA001046

Svensen, H., 2004. Release of methane from a volcanic basin as a mechanism for initial Eocene global warming. Nature 429, 542-545.

Taylor, K.W.R., Huber, M., Hollis, C.J., Hernandez-Sanchez, M.T., Pancost, R.D., 2013. Re-evaluating modern and Palaeogene GDGT distributions: Implications for SST reconstructions. Global and Planetary Change 108, 158-174.

Tierney, J.E., Tingley, M.P., 2014. A Bayesian, spatially-varying calibration model for the TEX_{86} proxy. Geochimica et Cosmochimica Acta 127, 83-106.

Villasante-Marcos, V., Hollis, C.J., Dickens, G.R., Nicolo, M.J., 2009. Rock magnetic properties across the Paleocene-Eocene Thermal Maximum in Marlborough, New Zealand. Geologica Acta 7(1/2), 229-242.

Wilkinson, B.H., Algeo, T.J., 1989. The sedimentary carbonate record of calcium magnesium cycling. American Journal of Science 289, 1158-1194.

Zachos, J.C., Stott, L.D., Lohmann, K.C., 1994. Evolution of early Cenozoic marine temperatures. Paleoceanography 9, 353-387.

Zachos, J.C., Pagani, M., Sloan, L.C., Thomas, E., Billups, K., 2001. Trends, rhythms, and aberrations in global climate 65[thinsp]Ma to present. Science 292, 686-693.

Zachos, J.C., Wara, M.W., Bohaty, S., Delaney, M.L., Petrizzo, M.R., Brill, A., Bralower, T.J., Premoli-Silva, I., 2003. A transient rise in tropical sea surface temperature during the Paleocene-Eocene thermal maximum. Science 302, 1551-1554.

Zachos, J.C., Röhl, U., Schellenberg, S.A., Sluijs, A., Hodell, D.A., Kelly, D.C., Thomas, E., Nicolo, M., Raffi, I., Lourens, L.J., McCarren, H. , Kroon, D. , 2005. Rapid acidification of the ocean during the Paleocene-Eocene Thermal Maximum. Science 308, 1611-1615.

Zachos, J.C., Schouten, S., Bohaty, S., Quattlebaum, T., Sluijs, A., Brinkhuis, H., Gibbs, S.J., Bralower, T.J., 2006. Extreme warming of mid-latitude coastal ocean during the Paleocene-Eocene Thermal Maximum: Inferences from TEX_{86} and isotope data. Geology 34, 737-740.

Zachos, J.C., Dickens, G.R., Zeebe, R.E., 2008. An early Cenozoic perspective on greenhouse warming and carbon-cycle dynamics. Nature 451, 279-283.

Zachos, J.C., McCarren, H., Murphy, B., Röhl, U., Westerhold, T., 2010. Tempo and scale of late Paleocene and early Eocene carbon isotope cycles: Implications for the origin of hyperthermals. Earth and Planetary Science Letters 299, 242-249.

FIGURES

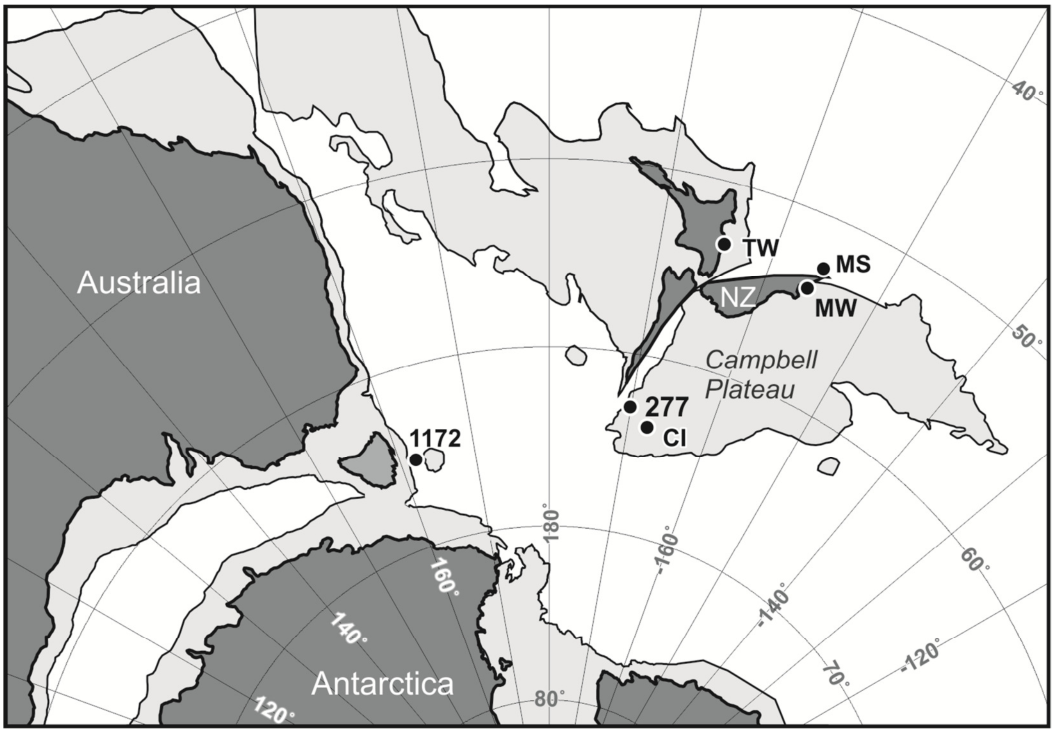

Figure 1. Location of DSDP Site 277 on a tectonic reconstruction for the southwest Pacific during the early Eocene (~54 Ma) (after Cande and Stock, 2004). Other localities mentioned in the text are also shown: ODP Site 1172, Campbell Island (CI), Tawanui (TW), Mid-Waipara River (MW) and Mead Stream (MS).

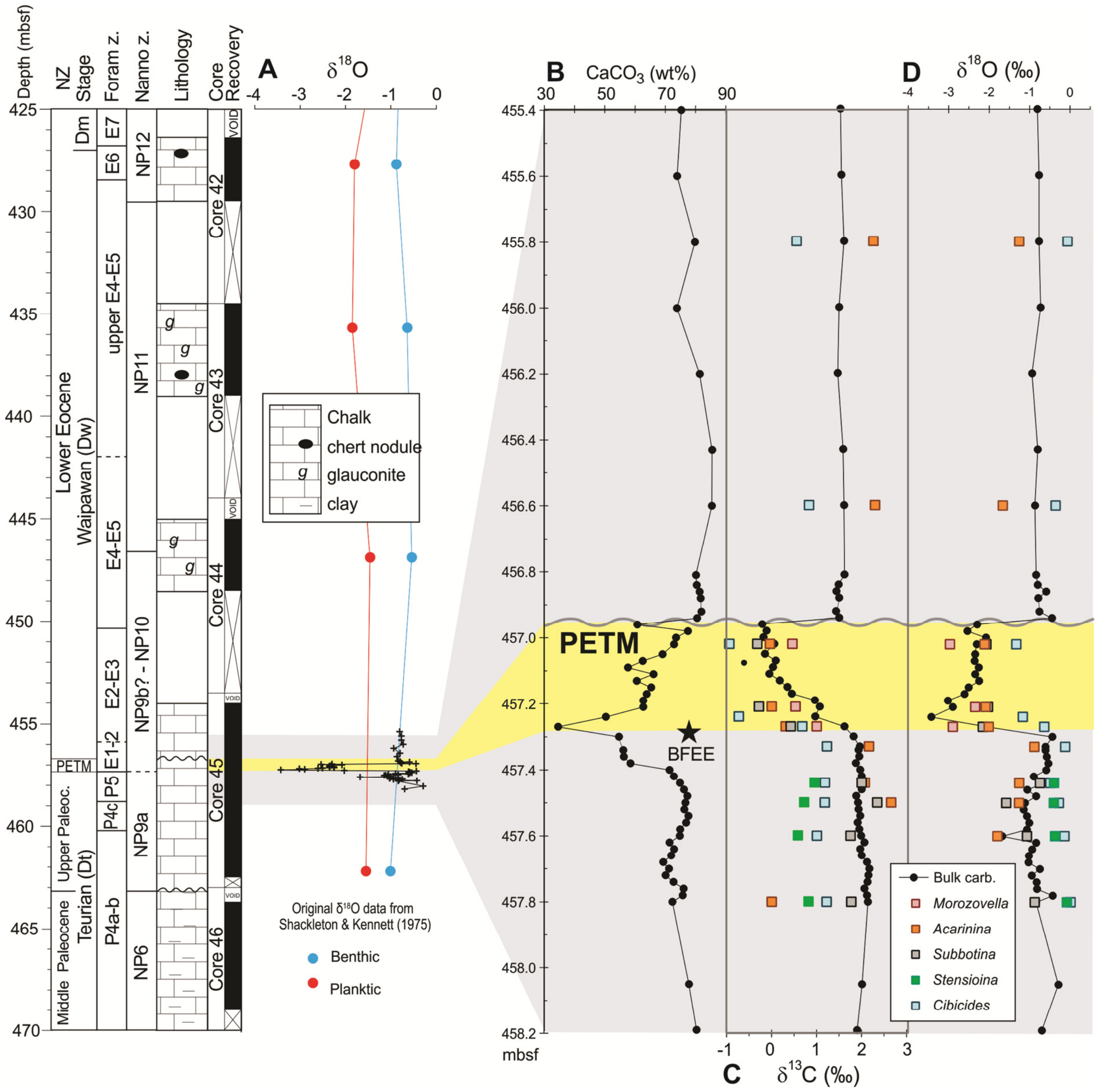

Figure 2. Biostratigraphy, lithologies, carbonate content (B) and stable isotopes from bulk carbonate and foraminifera (A, C, D) across the Paleocene-Eocene transition at DSDP Site 277. Abbreviations: Mangaorapan local stage (Dm); Paleocene Eocene Thermal Maximum (PETM), Benthic Foraminiferal Extinction Event (BFEE). In (A) the new bulk carbonate $\delta^{18}O$ record is plotted alongside the uncorrected, mixed planktic and benthic $\delta^{18}O$ values of Shackleton and Kennett (1975); in (D) and subsequent figures, benthic $\delta^{18}O$ values include a correction factor of 0.28‰ (Katz et al., 2003).

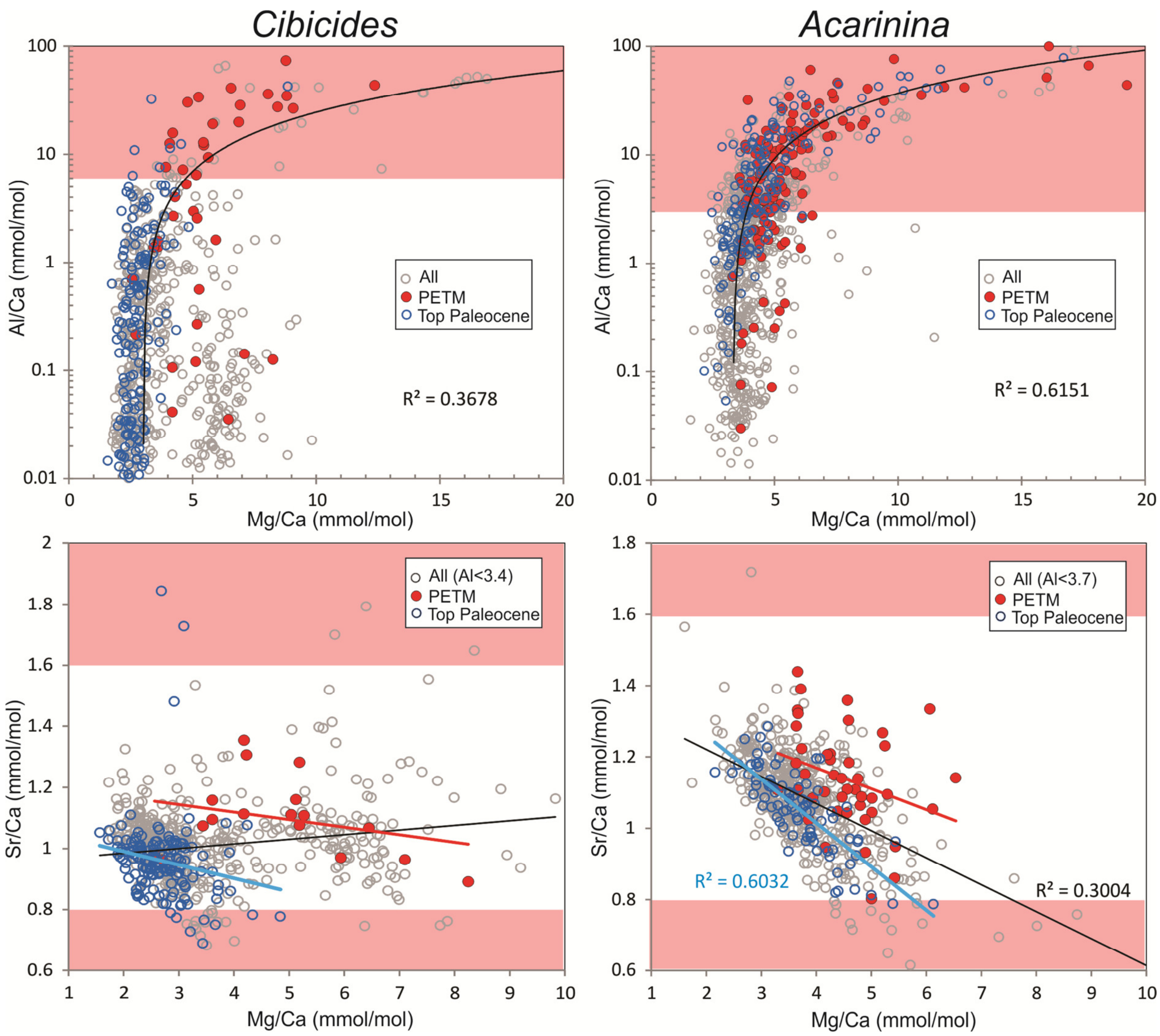

Figure 3. Cross-plots of Mg/Ca, Al/Ca and Sr/Ca with areas outside the screening limit shaded pink. All results are shown for the Al/Ca−Mg/Ca cross plots. For Sr/Ca−Mg/Ca cross plots, we only include measurements that lies within the screening limit for Al/Ca in order to exclude the effects of silicate contamination. Only R^2 values significant at the 95% confidence interval are shown for the trend lines.

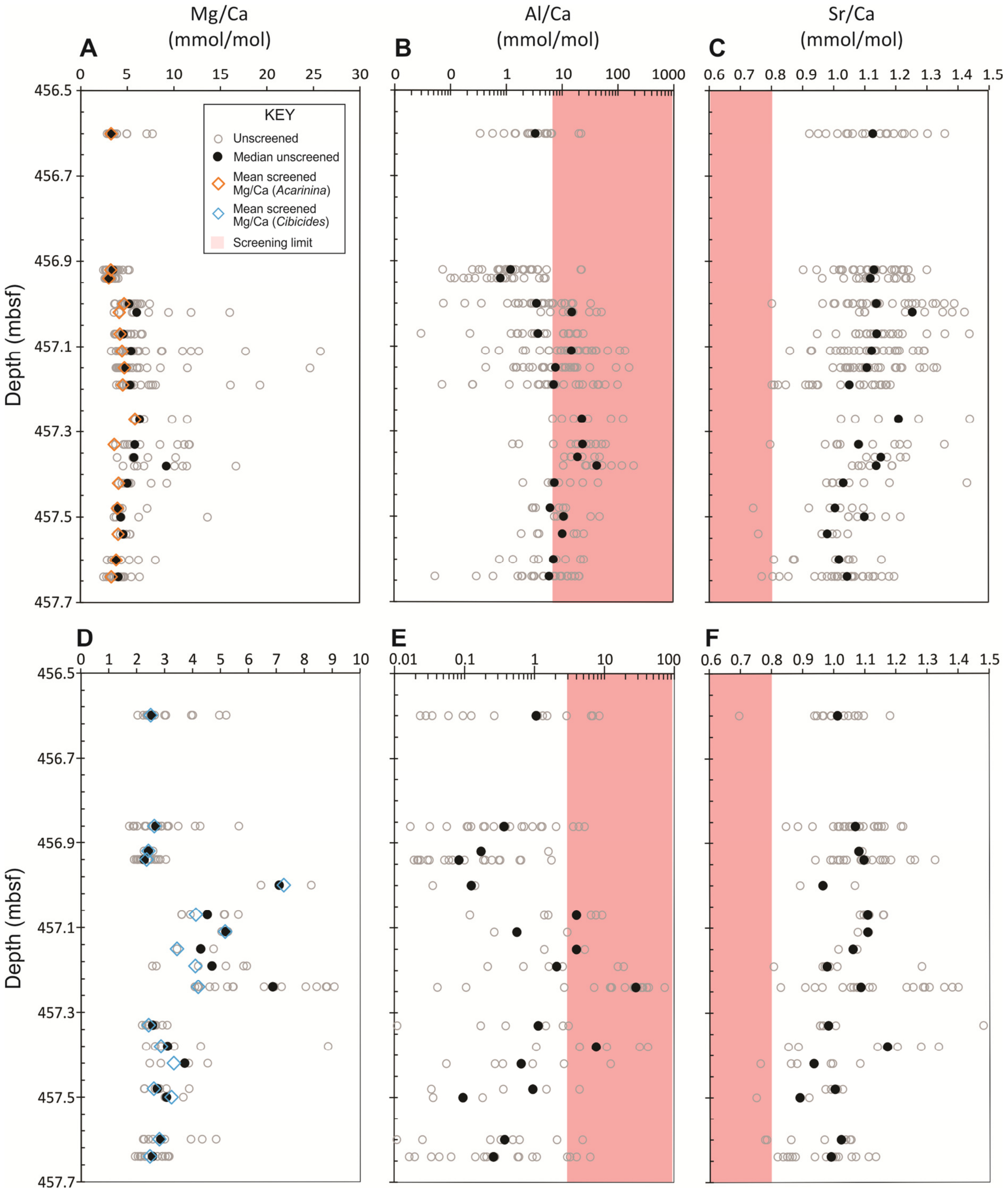

Figure 4. Trace element–depth plots for *Acarinina* (A−C) and *Cibicides* (D−F) across the PETM interval, showing all measured Mg/Ca, Al/Ca and Sr/Ca values, and the decrease in mean Mg/Ca value when Al/Ca and Sr/Ca screening protocols are imposed. Areas outsides the screening limits are shaded pink. Note change in scale on horizontal axes for Mg/Ca and Al/Ca for *Acarinina* and *Cibicides*.

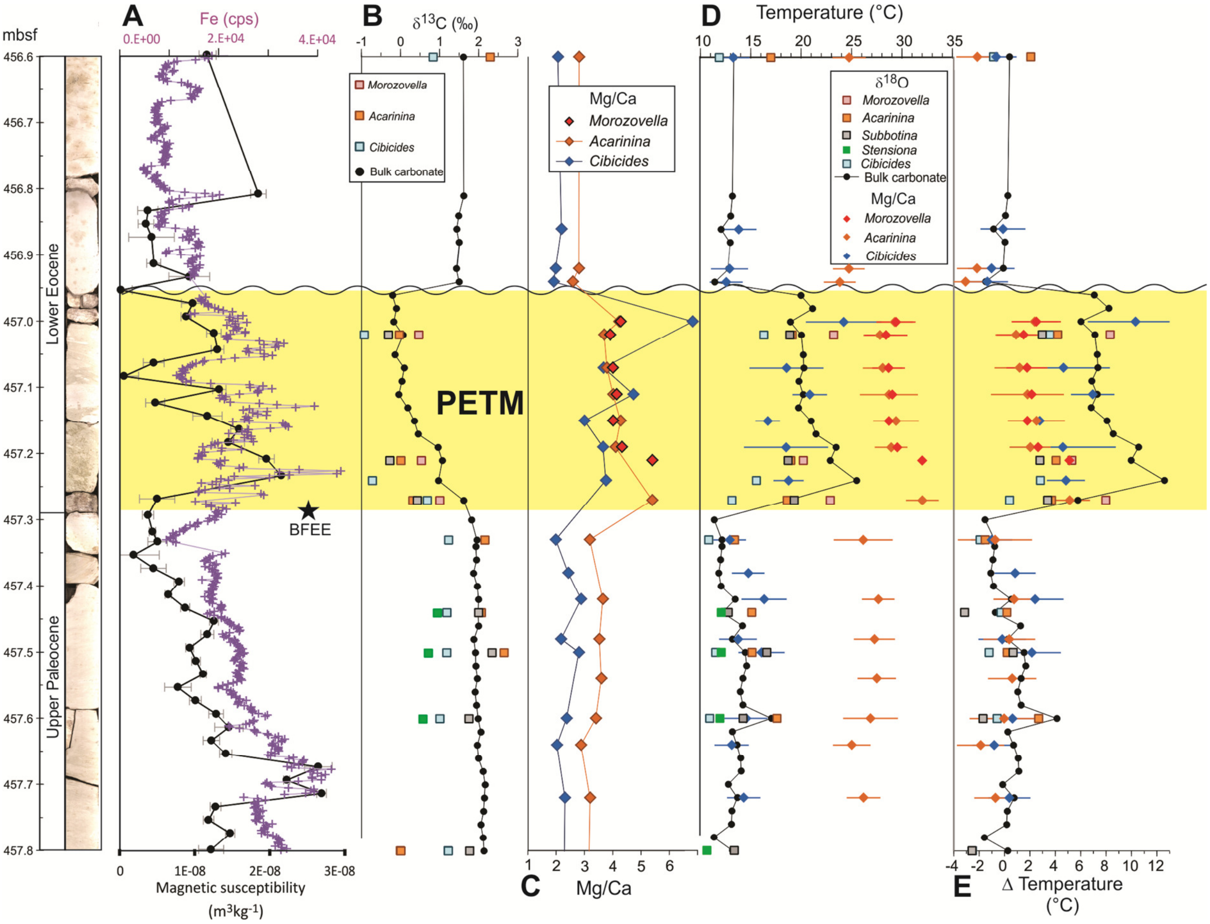

Figure 5. Variation in (A) Fe content and magnetic susceptibility; (B) δ^{13}C; (C) Mg/Ca ratios; (D) paleotemperatures derived from δ^{18}O values and Mg/Ca ratios; and (E) changes in paleotemperature relative to average Paleocene values.

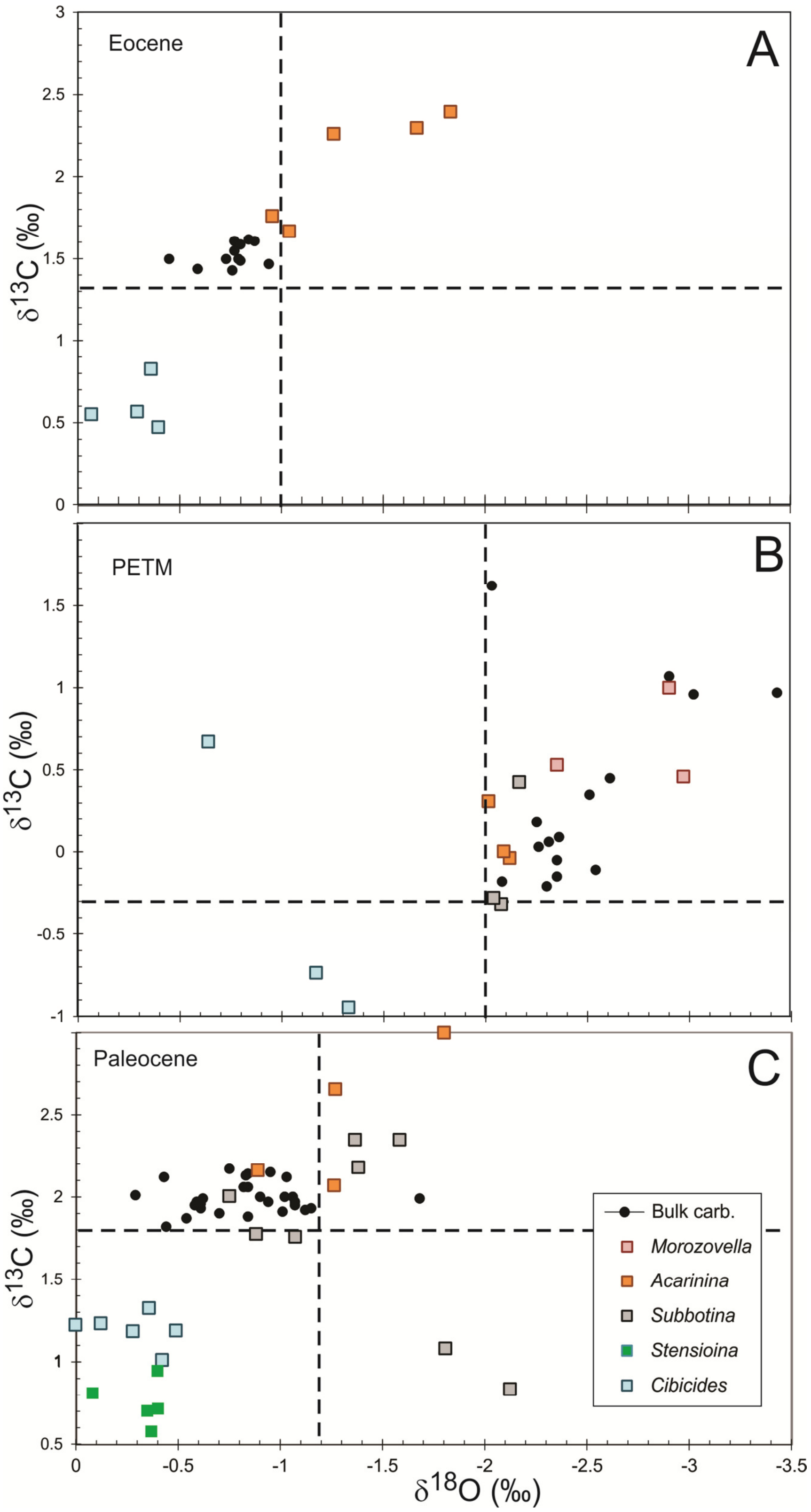

Figure 6. Cross plot of stable isotope ($\delta^{13}C$, $\delta^{18}O$) values for bulk carbonate, *Cibicides*, *Acarinina* and *Morozovella* within the Paleocene, Paleocene Eocene Thermal Maximum (PETM), and overlying Eocene.

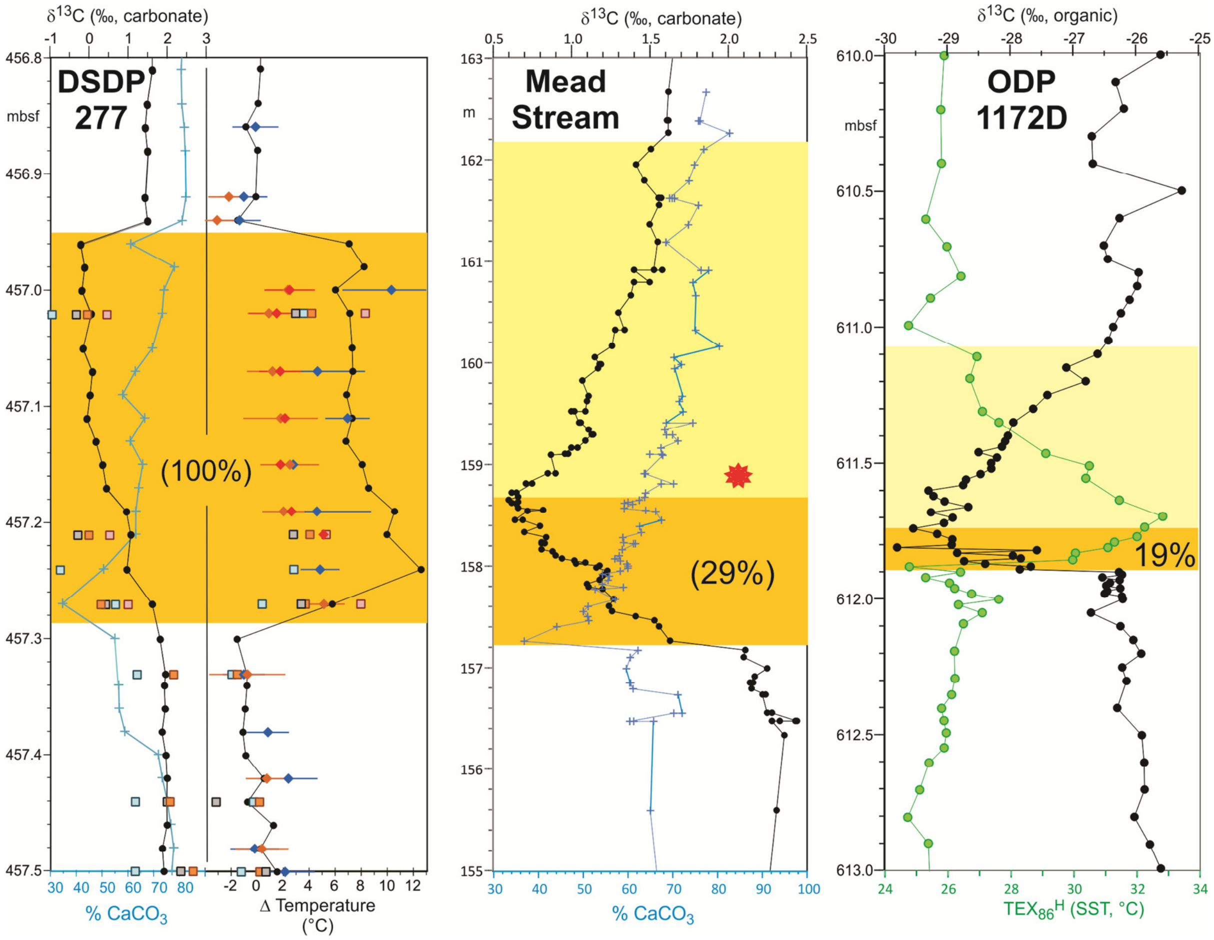

Figure 7. Comparison of records of the Paleocene–Eocene thermal maximum (PETM) at DSDP Site 277, ODP Site 1172 and Mead Stream. Symbols for DSDP Site 277 as in Fig. 4. Note the bulk carbonate $\delta^{18}O$ record is not plotted as a guide for relative temperature change at DSDP 277 because the record is inferred to be affected by diagenesis. The Red star marks a single occurrence of low-latitude radiolarians in the P-E transition interval at Mead Stream (Hollis, 2006).